

Giant resonances at complex excitation energies

J. R. Shepard, D. S. Oakley, and R. J. Peterson

University of Colorado, Boulder, Colorado 80309

(Received 14 July 1989)

We discuss the continuum response of finite nuclei in the giant resonance region in the context of a nonspectral random-phase approximation which straightforwardly includes correct continuum boundary conditions. Strongly collective discrete low-energy excitations of the nucleus are associated with poles with large residues in the random phase approximation particle-hole propagator at real excitation energies. Giant resonances, by comparison, are associated with similar poles at complex excitation energies where the imaginary part of the pole position corresponds to the escape width of the excitation. We illustrate these points with calculations of the isoscalar quadrupole response in ^{40}Ca . Here giant resonances are readily identified as sharp peaks in the particle-hole propagator in the complex excitation energy plane and the relation of the peaks to the continuum response (for real excitation energies) is demonstrated. Our numerical method allows extraction of transition densities for the giant resonances with continuum effects automatically included and these are used to compute (e, e') and (π, π') responses; illustrative comparisons with data are made.

I. INTRODUCTION

Collective excitations are familiar nuclear phenomena. Strong, low-lying quadrupole and octupole excitations are observed in nearly all nuclei and such excitations are well described by microscopic many-body theories such as the random-phase approximation (RPA). Similar collective phenomena are seen in the nuclear continuum in the form of giant resonances which appear in experimental spectra as broad and systematic features above some smoother background. Continuum excitations pose special problems both experimentally and theoretically. Apart from complications involving the separation of various multipoles of the nuclear response, empirical information about giant resonances must be extracted from the broad peaks after subtraction of the background. Theoretical treatments are complicated by the necessity of including the dynamics of the continuum correctly. For example, while correct treatment of continuum boundary conditions is not likely to be a problem in the one-particle-one-hole (p-h) RPA description of discrete low-lying states, these boundary conditions are essential for a proper description of the escape widths of resonant excitations. Passing from the discrete-basis RPA to a full continuum RPA (especially when finite-range nucleon-nucleon interactions are employed) requires fundamental changes in the calculational approach. Furthermore, in the discrete approach, the nuclear response is built up from nonoverlapping contributions of individual excitations whose own response is readily factored into products of transition densities. These in turn can be used in standard reaction codes to generate the observables of scattering processes. In contrast, for continuum calculations, various resonances overlap and a smooth background is present which does not allow, in any obvious way, the useful factorization possible in the discrete case. This means that it is not obvious even how precisely to

define a giant resonance; for example, we cannot readily identify its transition density in the same way as for a discrete excitation.

In this paper, we examine the continuum RPA p-h propagator (or polarization insertion) for ^{40}Ca based on a relativistic quantum hydrodynamic (QHD-1) mean-field-theory (MFT) ground state. The p-h propagator is evaluated for complex excitation energies, ω , and giant resonance contributions to the nuclear response are identified with poles in the p-h propagator in the complex ω plane. This picture provides a clear theoretical working definition of what a giant resonance is and permits direct extraction of a transition density for the giant resonance even when continuum effects contributing to the escape width are included. Although the calculations to be described below are based on a relativistic model of nuclear structure, the points we wish to stress are quite general and apply to any continuum-RPA treatment. Furthermore, while we restrict our attention to 1p-1h RPA, the picture of the nuclear response that emerges shows how 2p-2h contributions may be readily included in an approximate way.

II. NONSPECTRAL DIRAC RPA

QHD-1 (Ref. 1) is a relativistic field-theoretic model of nuclear dynamics based on the interaction of a nucleon field with an attractive scalar-isoscalar σ -meson field and a repulsive vector-isoscalar ω -meson field. The mean-field approximation in this model has been shown² to provide a good description of the properties of the ground states of doubly magic nuclei with few free parameters. A random-phase-approximation (RPA) calculation based on this mean-field theory (MFT) has recently been developed³⁻⁹ for the description of 1p-1h excitations in the doubly magic nuclei. These RPA calculations give rise to exactly conserved transition currents as well as an exact treatment of spuriousity in $1^- T=0$ excitations.

They also account quite well for low-lying collective excitations⁴⁻⁷ and can also give a reasonable description of the electron scattering Coulomb response in the quasi-elastic region.^{4,8,9} The calculations of Blunden and McCorquodale,³ which include isovector meson fields and exchange contributions, account quite well for all of the levels in ¹²C up to the 16.1 MeV $2^+ T=1$ state.

A variety of numerical techniques have been employed to solve the QHD-1 RPA and we now focus on the so-called “nonspectral” method^{4,8,9} in which the correct continuum boundary conditions may straightforwardly be included. A schematic discussion of this method begins with the single-particle propagator (or Green function) of the MFT:

$$G_{\text{MF}} = G_0 + G_0 \Sigma_{\text{MF}} G_{\text{MF}}, \quad (2.1)$$

where the MFT propagator G_{MF} is expressed in terms of the free propagator G_0 and the self-consistent MFT self-energy, Σ_{MF} . The quantity G_{MF} has (at least) two entirely equivalent forms. The more familiar is the “spectral” representation:

$$G_{\text{MF}}(\mathbf{x}, \mathbf{y}; \omega) = \sum_{\beta} \psi_{\beta}(\mathbf{x}) \bar{\psi}_{\beta}(\mathbf{y}) G_{\beta}(\omega), \quad (2.2)$$

where

$$G_{\beta}(\omega) = \frac{\theta(\epsilon_{\beta} - \epsilon_F^+)}{\omega - \epsilon_{\beta} + i\eta} + \frac{\theta(\epsilon_F - \epsilon_{\beta})}{\omega - \epsilon_{\beta} - i\eta}, \quad (2.3)$$

and where ψ_{β} is an eigenfunction with eigenvalue ϵ_{β} of the single-particle Dirac equation containing the potential Σ_{MF} . The Fermi energy ϵ_F is the eigenvalue of the highest-energy occupied orbital. As is evident from Eqs. (2.2) and (2.3), G_{MF} has poles at the eigenenergies and residues equal to the outer product of the associated eigenfunctions. G_{MF} may also be expressed in nonspectral form:¹⁰

$$G_{\text{MF}}(\mathbf{x}, \mathbf{y}; \omega) = \sum_{ljm} [\psi_{u;ljm}(\mathbf{x}; \omega) \bar{\psi}_{v;ljm}(\mathbf{y}; \omega) \theta(y - x) + \psi_{v;ljm}(\mathbf{x}; \omega) \bar{\psi}_{u;ljm}(\mathbf{y}; \omega) \theta(x - y)], \quad (2.4)$$

where $\psi_u(\omega)$ and $\psi_v(\omega)$ satisfy the same Dirac equation as the ψ_{β} but with $\epsilon_{\beta} \rightarrow \omega$ and where ψ_u is regular at the origin while ψ_v is regular at large distances. The nonspectral form of G_{MF} provides a practical method for proper treatment of the continuum (or continua—for both positive and negative energies—in the present QHD case) which is not feasible using the spectral expression.

The particle-hole propagator for the MFT ground state is defined schematically as

$$\Pi_{\text{MF}}(\omega) = i \int \frac{d\omega'}{2\pi} G_{\text{MF}}(\omega + \omega') G_{\text{MF}}(\omega'). \quad (2.5)$$

After dropping vacuum-vacuum contributions,⁴ the spectral form of G_{MF} [Eqs. (2.2) and (2.3)] may be used to write

$$\Pi_{\text{MF}}(\mathbf{x}, \mathbf{y}; \omega) = - \sum_{\alpha} \sum_{\epsilon_F \geq \beta > 0} \left[\frac{\bar{\mathcal{F}}_{\alpha\beta}(\mathbf{x}) \mathcal{F}_{\alpha\beta}(\mathbf{y})}{\omega - \omega_{\alpha\beta} + i\eta} - \frac{\bar{\mathcal{F}}_{\beta\alpha}(\mathbf{x}) \mathcal{F}_{\beta\alpha}(\mathbf{y})}{\omega + \omega_{\alpha\beta} - i\eta} \right], \quad (2.6)$$

where $\omega_{\alpha\beta} \equiv \epsilon_{\alpha} - \epsilon_{\beta}$ and the single-particle transition densities are defined by

$$\mathcal{F}_{\alpha\beta}(\mathbf{x}) \equiv \psi_{\beta}(\mathbf{x}) \bar{\psi}_{\alpha}(\mathbf{x})$$

and

$$\bar{\mathcal{F}} = \gamma^0 \mathcal{F}^{\dagger} \gamma^0. \quad (2.7)$$

Evidently, Π_{MF} has poles at the unperturbed p-h excitation energies and the residue at these poles is the outer product of the associated transition densities. Note that the 1p-1h matrix element of a one-body operator \mathcal{O} is

$$\langle \mathcal{O} \rangle_{\text{ph}} = \int d^3r \text{Tr}[\mathcal{O}(\mathbf{r}) \mathcal{F}_{\text{ph}}(\mathbf{r})] = \langle \psi_p | \mathcal{O} | \psi_h \rangle.$$

The RPA is embodied in the schematic integral relation

$$\Pi_{\text{RPA}} = \Pi_{\text{MF}} + \Pi_{\text{MF}} K \Pi_{\text{RPA}}, \quad (2.8)$$

where Π_{RPA} is the correlated RPA particle-hole propagator and K is the interaction kernel which depends on the meson masses and meson-nucleon-nucleon coupling constants. Using the spectral form of Π_{MF} , the integral equation for Π_{RPA} becomes the familiar pair of matrix eigenvalue equations [see, e.g., Eq. (4.5) of Ref. 4]. Quite generally, we can express Π_{RPA} in the Lehmann representation¹¹ and the result has the same form as Eq. (2.6) except $\omega_{\alpha\beta} \rightarrow \omega_n$ and $\mathcal{F}_{\alpha\beta} \rightarrow \mathcal{F}^{(n)}$ where n labels the n th RPA phonon. In Ref. 4 the integral form of the RPA equation is solved directly, and low-lying discrete excitations are identified as singularities in Π_{RPA} at $\omega = \omega_n$, real. The residues at these poles are obtained numerically and the associated RPA transition density $\mathcal{F}^{(n)}$ can then be extracted. The transition densities then yield matrix elements of one-body operators and observables for processes like inelastic electron scattering. Comparison of excitation energies and electron-scattering form factors computed in large-basis spectral RPA calculations^{6,7} with calculations using the nonspectral method⁴ shows that the two methods are essentially equivalent for discrete excitations.

The linear response of a nucleus to a probe whose interaction vertex with a nucleon is represented by the operator \mathcal{O} is expressed quite generally in terms of Π_{RPA} via

$$S_{\mathcal{O}}(\omega) = - \frac{1}{\pi} \text{Im} \text{Tr}[\mathcal{O} \Pi_{\text{RPA}}(\omega) \mathcal{O}]. \quad (2.9)$$

For discrete excitations, a simpler factorized expression is obtained:

$$S_{\mathcal{O}}(\omega) = \sum_n |\langle \mathcal{O} \rangle^{(n)}|^2 \delta(\omega - \omega_n), \quad (2.10)$$

where

$$\langle \mathcal{O} \rangle^{(n)} \equiv \text{Tr}[\mathcal{O}\mathcal{F}^{(n)}]. \quad (2.11)$$

By construction, the *spectral* form of the nuclear response takes on this form for all ω . In the *nonspectral* calculations, the factorizable form of the response is not directly applicable above particle threshold where the analytic structure of $\Pi_{\text{RPA}}(\omega)$ no longer is given by individual poles on the real axis. The continuum response must be computed directly using Eq. (2.9). This is numerically much more complicated than the evaluation of individual transition matrix elements, $\langle \mathcal{O} \rangle^{(n)}$, as is sufficient in the spectral method. For example, full distorted-wave impulse approximation calculations of (p,p') observables are routine for discrete excitations since several computer codes^{12,13,16,18} exist which can be used to evaluate the (p,p') form of $\langle \mathcal{O} \rangle^{(n)}$ given $\mathcal{F}^{(n)}$. In contrast, owing to the complicated structure of \mathcal{O} (involving, e.g., the NN t matrix and distorted waves), direct evaluation of the continuum response at an equivalent level of approximation using Eq. (2.9) has never been done. Only after further severe approximations has the (p,p') RPA continuum response been calculated.¹⁴ In general, there is no way around this difficulty. However, in the following section, we will outline a method of treating giant resonances in the nonspectral form which properly includes continuum effects and yet possesses the simplicities associated with discrete excitations.

III. CONTINUUM RESPONSE IN THE NONSPECTRAL METHOD

The spectral form of G_{MF} [Eqs. (2.2) and (2.3)] makes it clear that G_{MF} has poles at the real single-particle eigenvalues, ϵ_β . This form, however, is strictly applicable only to bound states. In practice, this difficulty is often circumvented by “putting the system in a box,” in which case continuum states are discretized and take the form of standing waves inside the box. As is well known,¹⁵ when the correct continuum boundary conditions are retained, the single-particle propagator will have poles at *complex* ω below the real axis which correspond to resonant single-particle levels. If we express the position of such a pole as $\epsilon_\alpha - i\Gamma_\alpha/2$, the width of the resonance is of course given by Γ_α . This behavior is implicitly present in the nonspectral form of G_{MF} given in Eq. (2.4). We now recall that Π_{MF} [Eq. (2.6)] has poles at $\epsilon_\alpha - \epsilon_\beta$ where $\epsilon_\alpha(\epsilon_\beta)$ is the eigenenergy of the particle (hole) single particle state. If Π_{MF} is computed using the spectral form of G_{MF} , and if α labels a *resonant* single-particle state, Π_{MF} will have a pole at a complex frequency,

$$\omega_{\alpha\beta} = \epsilon_\alpha - \epsilon_\beta - i\Gamma_\alpha/2.$$

Again, the residue at the pole will be given by the outer product of the single-particle transition density $\mathcal{F}_{\alpha\beta} = \psi_\beta \bar{\psi}_\alpha$, where ψ_α is the unbound resonant single-particle “wave function” defined in terms of the residue of G_{MF} for $\omega \rightarrow \epsilon_\alpha - i\Gamma_\alpha/2$. The response defined using the MFT analog of Eq. (2.9) will contain a contribution due to the pole at $\omega_{\alpha\beta}$ given by

$$\begin{aligned} S_{\mathcal{O}}^{\alpha\beta}(\omega) &= |\langle \mathcal{O} \rangle_{\alpha\beta}|^2 \left[-\frac{1}{\pi} \right] \text{Im} \left[\frac{1}{\omega - \omega_{\alpha\beta}} \right] \\ &= |\langle \mathcal{O} \rangle_{\alpha\beta}|^2 \frac{\Gamma_\alpha/2\pi}{[\omega - (\epsilon_\alpha - \epsilon_\beta)]^2 + (\Gamma_\alpha/2)^2}, \end{aligned} \quad (3.1)$$

where $\langle \mathcal{O} \rangle_{\alpha\beta} = \text{Tr}[\mathcal{O}\mathcal{F}_{\alpha\beta}]$. Thus this partial response looks just like the discrete response of Eq. (2.10) except that the δ function has been replaced by a Breit-Wigner distribution of strength. The discrete case is, of course, recovered in the limit $\Gamma_\alpha \rightarrow 0$.

IV. GIANT RESONANCES IN NONSPECTRAL DIRAC RPA

We have now outlined an approach in which resonances in the uncorrelated nuclear continuum can be thought of as singularities of the unperturbed particle-hole propagator in the complex ω plane. We anticipate that this will persist when RPA correlations are included but that the pole positions and residues of Π_{RPA} will differ from those of Π_{MF} . More specifically, we expect that giant resonances will appear as poles in Π_{RPA} with particularly large residues just as RPA correlations concentrate transition strength in low-lying discrete collective levels.

To investigate this question we have evaluated the nonspectral isoscalar quadrupole QHD-1 MFT RPA particle-hole propagator for ^{40}Ca using the calculational methods outlined in Ref. 4. The “finite Hartree” coupling constants and meson masses presented in Table V of Ref. 1 were employed. This RPA propagator was evaluated using the code DRPA (Refs. 4 and 26) at a grid of points in the complex ω plane in the region $10 \leq \text{Re } \omega \leq 35$ MeV and $0.1 \leq -\text{Im } \omega \leq 7$ MeV. In Fig. 1 we show a three-dimension plot of the quantity

$$|\Pi_{\text{RPA}; J=2^+, T=0}^{11;11}(x_0, x_0; \omega)|, \quad (4.1)$$

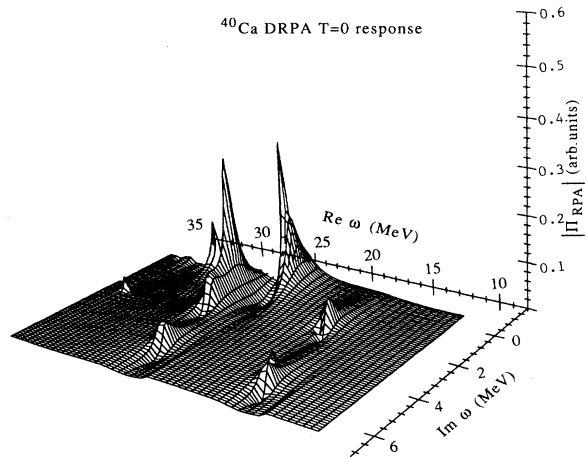


FIG. 1. Π_{RPA} [expression (4.1)] for ^{40}Ca $T=0$, $J^\pi=2^+$ in complex ω plane.

TABLE I. ^{40}Ca $T=0$ GQR strengths extracted from the DRPA poles versus the values extracted from fits to the response spectra of Fig. 3.

Peak	ω (MeV)	Γ (MeV)	Response from poles (% of peak 2)	Response $q=150$ MeV/c fit (% of peak 2)	Response $q=450$ MeV/c fit (% of peak 2)
1	16.8	5.0	20	0	25
2	22.3	1.7	100	100	100
3	25.4	3.4	90	6	70
4	29.8	0.7	36	5	47
5	33.5	5.6	1	1	51

where 11;11 is a Dirac index label explained in Ref. 4 and where x_0 is a matching radius roughly corresponding to the radius of the nucleus. This plotted quantity shows directly the pole structure of the particle-hole propagator, Π_{RPA} . As is evident from Fig. 1 this quantity is highly structured with sharp peaks at points in the ω plane listed in Table I. We identify each of the peaks as a numerical approximation to poles in Π_{RPA} , which in turn we associate with individual components of the isoscalar quadrupole giant resonance. This association is established by examining the isoscalar component of the ^{40}Ca response presented in Fig. 2. In this figure, the RPA response at a momentum transfer of 150 MeV/c calculated directly using Eq. (2.9) is the solid line. According to the interpretation previously outlined, this response should consist of peaks corresponding to the structures seen in Fig. 1 and having widths given by the distance of

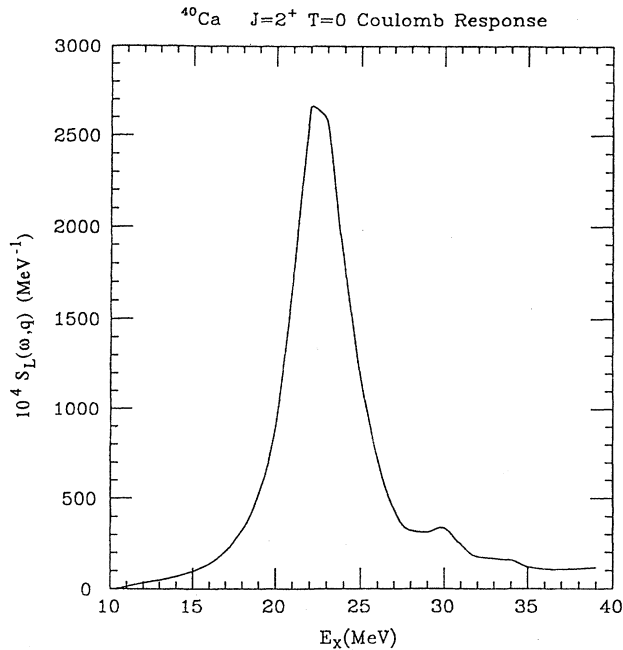


FIG. 2. ^{40}Ca $T=0$, $J^\pi=2^+$ RPA response versus excitation energy ($\text{Re } \omega$, MeV) at a momentum transfer of $q=150$ MeV/c. An artificial spreading of 2 MeV is included for display purposes.

these structures from the real axis. These resonant contributions rise on a nonresonant background without sharp structure in the complex ω plane.

The appropriateness of this interpretation is indicated in Fig. 3, where a decomposition of the computed $\Delta T=0$ response in terms of Breit-Wigner peaks riding on a smooth background has been made. This decomposition assumes the Breit-Wigner shapes to have centroids and widths approximately corresponding to the complex ω values of the resonant structures shown in Fig. 1 and listed in Table I. The overall strength of each peak in the response was determined by a best-fit procedure and is also listed in Table I. Figure 3 shows that this decompo-

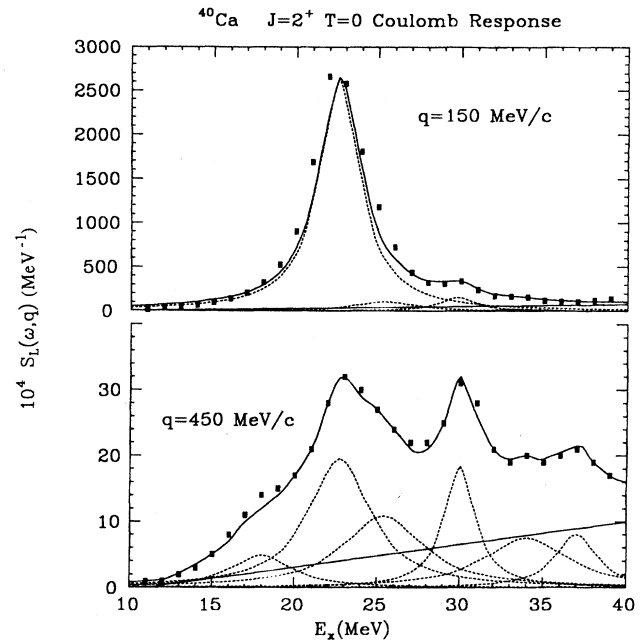


FIG. 3. Peak-fitting analysis of response spectra. The points represent calculations as in Fig. 2, the dotted lines are the fitted curves, the lower solid line is a background, and the solid line is the sum of the fits and background. In this fitting procedure the peak locations and widths were allowed to vary by 10% from those of Table I. Because of the dependence of the response on momentum transfer, we show a spectrum at $q=150$ MeV/c (top, as in Fig. 2) and at $q=450$ MeV/c (bottom). As before, an artificial spreading of 2 MeV is included for display purposes.

sition gives an excellent reproduction of the full response. Furthermore, the response of each peak, as determined by fitting and tabulated in Table I, coincides very well with the numerically determined *residue* of the corresponding singularity in the quantity defined in expression (4.1) and displayed in Fig. 1. This leads to a working definition of a giant resonance as a singularity of the particle-hole propagator with a large residue which is analogous to an ordinary discrete collective excitation in every way except that this singularity appears at a complex frequency rather than a real one. Furthermore, the imaginary part of the pole position corresponds to the escape width of the resonance. While RPA correlations shift the energy and alter the strength of simple particle-hole (or MFT) discrete excitations, they may also affect the *width* of resonances by shifting their poles vertically in the complex ω plane. Evidence for this is presented in Fig. 4 where the uncorrelated (or MFT) analog of the quantity defined in expression (4.1) and shown in Fig. 1 is displayed. The corresponding response appears in Fig. 5. The observed structures are quite different from those shown in Fig. 1. The most striking difference is the very strong peak in the RPA calculation at $\omega = 22.3 - i0.83$ MeV which gives the dominant contribution to the response in Fig. 2 and should perhaps be considered *the* isoscalar quadrupole giant resonance.

V. COMPARISON WITH EXPERIMENT

We have suggested here that a giant resonance be defined as a “strong” singularity of the particle-hole propagator at a complex frequency. It is not our main purpose in this paper to stress comparison with experiment but rather to establish a framework for future comparisons when more complete calculations of this kind become available. Nevertheless, we now make some preliminary comparisons to illuminate further the specifics of our approach.

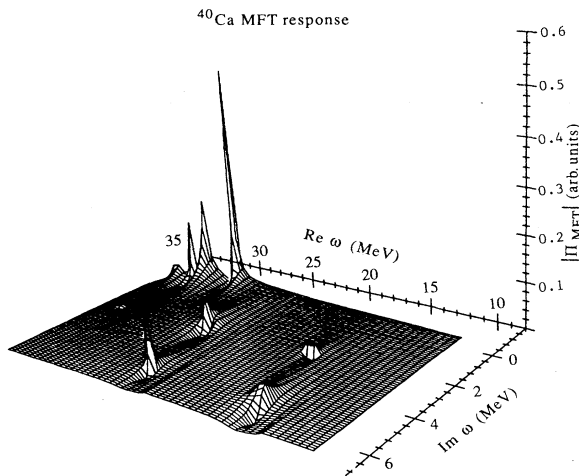


FIG. 4. Π_{MFT} [expression (4.1)] for ^{40}Ca $T=0$, $J^\pi=2^+$ in complex ω plane.

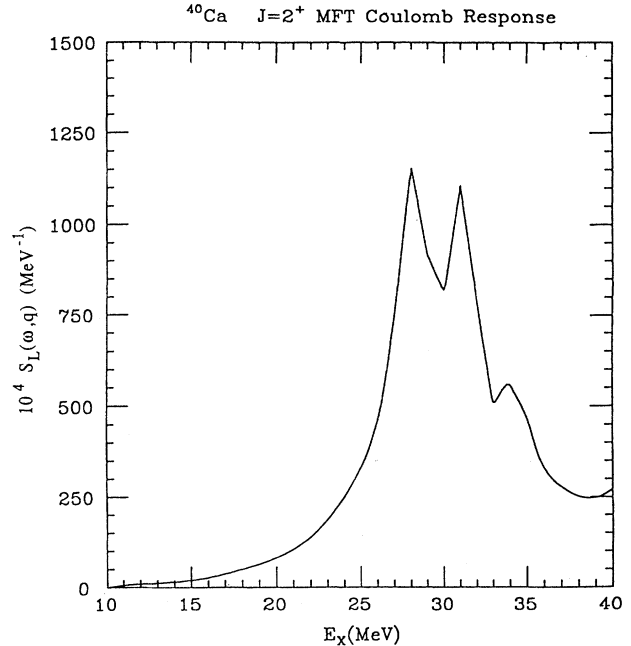


FIG. 5. ^{40}Ca $T=0$, $J^\pi=2^+$ MFT response versus excitation energy ($\text{Re } \omega$, MeV). An artificial spreading of 2 MeV is included for display purposes.

Because our numerical^{4,26} methods allow extraction of the residues for poles on or off the real axis, we may extract transition densities $\mathcal{F}_{\text{RPA}}^{(n)}$ for each resonant excitation just as we have done for discrete excitations. Figure 6 (top) shows the transition radial density [actually the quantity $\mathcal{F}_{L=J=2, S=0}^{11}(r)$ as defined in Ref. 4] extracted from the $T=0$ calculation for the resonances at $22.3 - i0.83$ and $29.8 - i0.35$ MeV. These quantities correctly include the continuum boundary conditions. The two transition densities have very different radial shapes which imply different q dependence in the (e, e') response [see Fig. 6 (bottom)], namely, the lower-energy resonance peaks at $q \approx 150$ MeV/c while the upper peaks at ~ 300 MeV/c. These transition densities may be used in, e.g., conventional distorted-wave codes^{12,13,16-18} with the understanding that the corresponding contribution to the response is given by the appropriate form of Eq. (3.1). For example, the contribution to the (π, π') response due to a particular resonance excitation would be

$$\frac{d^2\sigma^{(n)}}{d\omega d\Omega} = \frac{d\sigma^{(n)}}{d\Omega} \frac{\Gamma_n/2\pi}{(\omega - \omega_n)^2 + (\Gamma_n/2)^2}, \quad (5.1)$$

where the complex pole position for the resonance is $\omega_n - i\Gamma_n/2$ and where $d\sigma^{(n)}/d\Omega$ is the (π, π') cross section computed using the distorted-wave impulse approximation (DWIA). In Fig. 7 (top) we show such a calculation of $d\sigma^{(n)}/d\Omega$ for an isoscalar-quadrupole excitation in the $^{40}\text{Ca}(\pi, \pi')^{40}\text{Ca}$ reaction. These cross sections were obtained from the code DWPI (Ref. 17) using the neutron and proton transition densities extracted from the DRPA (Ref. 4) output for the resonance at $21.2 - i1.1$ MeV and

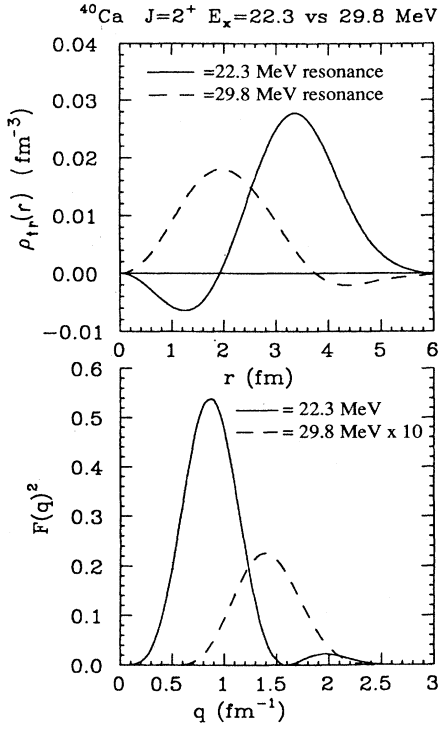


FIG. 6. Transition densities for 22.3 and 29.8 MeV quadrupole states. These are plotted versus radius (top) and momentum transfer (bottom).

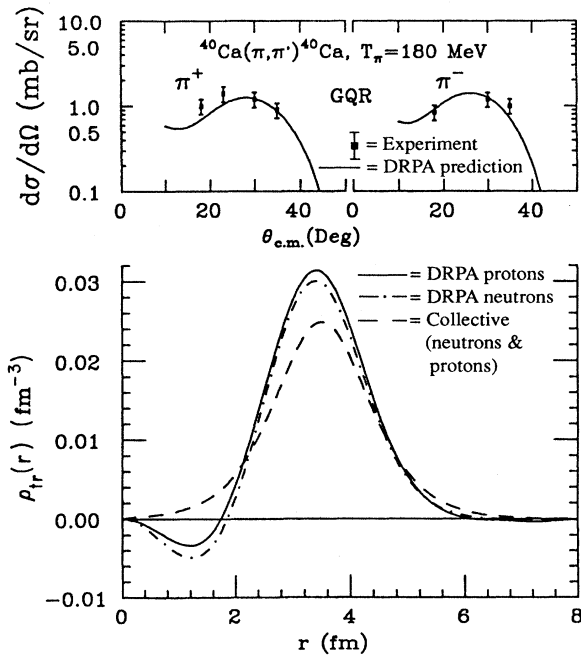


FIG. 7. Comparison (top) of $^{40}\text{Ca}(\pi, \pi')^{40}\text{Ca}$ GQR cross sections from experiment¹⁹ (data points) and the prediction of this work (solid curves). Comparison (bottom) of ^{40}Ca GQR transition densities extracted from this work (solid=proton, dot-dashed=neutron) and the collective density fitted to the data (dashes).

are compared with those extracted from the 22 MeV complex (identified as being dominantly isoscalar quadrupole in nature) observed in π^\pm inelastic scattering on ^{40}Ca by Ullmann *et al.*¹⁹ Here the pole is shifted slightly from the value of $22.3 - i0.83$ MeV quoted earlier because we have included the differences in neutron and proton wave functions and single-particle propagators due to Coulomb effects. These resultant radial-transition densities were employed in this DWIA calculation with pion distorted waves generated from ground-state distribution parameters taken from electron scattering while the pi-nucleon effective interactions were calculated from the phase shifts of Ref. 20.

As seen in Fig. 7 (top), the agreement between the data and calculation is excellent in both shape and magnitude for the π^- (neutronlike) as well as for π^+ (protonlike) cross sections. Note that no adjustment of the normalization has been made. This calculation of the location and width of this component of the isoscalar-quadrupole resonance is also in reasonable agreement with the pion-scattering results (Table II), particularly in light of the fact that the two-particle-two-hole effects (in the following) would tend to spread this peak further. A collective-model (Tassie) fit to these data, with transition densities proportional to the radial derivative of the ground-state density as given in Refs. 19 and 21, yields a $B(C2)\uparrow$ value of $170 \pm 25 e^2 \text{fm}^4$ while the $B(C2)\uparrow$ computed from our RPA transition density is $120 e^2 \text{fm}^4$. These quantities are compared with results from (e, e') and (α, α') measurements in Table II.^{22,23} The dominant Dirac component of our RPA radial-transition density⁴ is compared with the collective density in Fig. 7 (bottom) where both of these calculations, in spite of the differing $B(C2)\uparrow$ values, reproduce the observed cross sections. The computed RPA $B(C2)\uparrow$ value exhausts 26% of the classical isoscalar-charge sum rule while the data of Ullmann *et al.* account for $32 \pm 5\%$, if the Tassie model is assumed. The overall level of agreement between theory and experiment in Table II is quite good considering the model dependence and uncertainties inherent in all quantities. In spite of this reasonable agreement, we still wish to emphasize mainly the approach we have outlined and to indicate the kind of analyses which can be made in the future using more complete calculations.

TABLE II. Comparison of results from the Dirac-RPA predictions (with neutrons and protons treated separately) and experiment for ^{40}Ca isoscalar giant quadrupole.

	E_x (MeV)	Γ (MeV)	$B(C2)\uparrow$ ($e^2 \text{fm}^4$)
DRPA	21.2	2.2	120
(e, e') ^a	~ 17.5	~ 5	148 ± 20
(π, π') ^b	~ 22	~ 7	170 ± 25
(α, α') ^c	17.7	2.5	270 ± 11

^aFrom Ref. 22. Width estimated.

^bTaken from a collective fit to the π^- and π^+ data of Ref. 19. Width estimated.

^cFrom Ref. 23, using a collective model.

VI. TWO-PARTICLE-TWO-HOLE CORRECTIONS

One important shortcoming of the RPA approach presented here is the omission of two-particle-two-hole (2p-2h) effects which, for example, contribute to the spreading widths of the nuclear response. Treating such effects directly in a "second RPA" formulation is numerically very demanding.²⁴ Recently, Smith and Wambach²⁵ have developed an approximate treatment of 2p-2h effects which may readily be adapted to the methods outlined here. Smith and Wambach account for 2p-2h couplings via a complex, energy-dependent self-energy determined from empirical single-particle spreading widths. They argue that the *state* dependence of these self-energies may be approximated by a simpler spin-isospin channel dependence. Thus their treatment involves *four* self-energies, $\Sigma_{ST}(\omega)$, where $S, T=0$ or 1 . In the language of the present treatment, 2p-2h effects are incorporated by modifying the definition of the response [given in Eq. (2.9)] by

$$S_{\mathcal{O}}^{2p-2h}(\omega) \equiv -\frac{1}{\pi} \text{Im Tr} \{ \mathcal{O} \Pi_{\text{RPA}}[\omega + \Sigma(\omega)] \mathcal{O} \}, \quad (6.1)$$

where the self-energy appropriate to the spin-isospin character of the operator \mathcal{O} is used. In practice, this response is simply computed by evaluating Π_{RPA} at the appropriate point in the complex ω plane rather than on the real axis as in the standard 1p-1h RPA. Similarly, the contribution due to the n th resonance [see Eq. (5.1)] becomes

$$S_{\mathcal{O}}^{(n)}(\omega) \rightarrow |\langle \mathcal{O} \rangle_{\text{RPA}}^{(n)}|^2 \left[-\frac{1}{\pi} \right] \times \text{Im} \left[\frac{1}{\omega + \Sigma(\omega) - \omega_n + i\Gamma_n/2} \right], \quad (6.2)$$

where

$$\langle \mathcal{O} \rangle_{\text{RPA}}^{(n)} \equiv \text{Tr}[\mathcal{O} \mathcal{F}_{\text{RPA}}^{(n)}]$$

is the matrix element of \mathcal{O} for the n th RPA excitation which has pole position $\omega_n - i\Gamma_n/2$ and transition density $\mathcal{F}_{\text{RPA}}^{(n)}$. Clearly, the imaginary part of $\Sigma(\omega)$ combines with the escape width, $\Gamma_n/2$, to increase the overall width of the response and is identified with the spreading width. The real part of $\Sigma(\omega)$ simply shifts the centroid of the peak. (Note that in the specific treatment of Ref. 25 the authors conclude $\Sigma_{S=T=0}=0$. Hence the computed isoscalar quadrupole response is unaffected by 2p-2h contributions in their approximation.)

VII. SUMMARY AND CONCLUSIONS

We have examined the structure of the nonspectral 1p-1h propagator as a function of complex excitation energy, ω . As usual, low-lying discrete excitations appear as singularities in the propagator at real ω . The transition densities for the associated excitations may straightforwardly be extracted from residues at these singularities. Our nonspectral propagator correctly includes appropriate continuum boundary conditions and, in consequence, "resonant" excitations above particle threshold appear as singularities at *complex* ω below the real axis. The distance of the pole from the real axis determines the escape width of the excitation. Transition densities for these resonant excitations may again be extracted from the residues at the singularities. Such transition densities automatically include correct continuum boundary conditions.

It is well known that correlations such as those included in the RPA can concentrate certain kinds of transition strength in low-lying, collective, discrete excitations. These collective excitations correspond to singularities in, e.g., the RPA 1p-1h propagator at real ω having particularly large residues. In the nonspectral approach, such RPA correlations also produce singularities with large residues at *complex* excitation energies. We identify the associated excitations as giant resonances. Again, the distance of the singularity from the real axis yields the escape width of the resonance. Transition densities reflecting correct continuum boundary conditions may be readily computed and then used, for example, in conventional reaction codes just as is typically done for discrete excitations.

To illustrate how our approach may be used in practice, we have examined the QHD1-MFT (Ref. 4) isoscalar quadrupole response of ⁴⁰Ca. Several distinct "singularities" were observed in the 1p-1h propagator, Π_{RPA} , in the complex excitation-energy plane. Each of these singularities was straightforwardly identified with structures in the computed (e, e') isoscalar quadrupole Coulomb response. These identifications support the association of the singularities with resonant excitations, "giant" and otherwise. Radial transition densities were extracted for two of the strong resonances. For the lower of the two ($\omega_{\text{pole}} = 22.3 - i0.83$ MeV), the transition density was used to calculate both a value of $B(C2)\uparrow$ and π^{\pm} inelastic cross sections. Agreement with experimental quantities was found to be reasonable. Finally, we have discussed how approximate treatment of 2p-2h effects may readily be included in our approach.

ACKNOWLEDGMENTS

We would like to acknowledge useful interactions with K. Vaziri, R. Smith, and E. Rost. This work was supported in part by the U.S. Department of Energy (DOE).

- ¹B. D. Serot and J. D. Walecka, *Adv. Nucl. Phys.* **16**, 1 (1986).
- ²C. J. Horowitz and B. D. Serot, *Nucl. Phys.* **A368**, 503 (1981).
- ³P. G. Blunden and P. McCorquodale, *Phys. Rev. C* **38**, 1861 (1988).
- ⁴J. R. Shepard, E. Rost, and J. A. McNeil, University of Colorado Report NPL-1046, 1989.
- ⁵R. J. Furnstahl, *Phys. Lett.* **152B**, 313 (1985).
- ⁶R. J. Furnstahl, *Proceedings of the International Conference on Spin Observables of Nuclear Probes, Telluride, 1988* (Plenum, New York, 1989).
- ⁷R. J. Furnstahl and J. Dawson (private communication).
- ⁸K. Wehrberger and F. Beck, *Phys. Rev. C* **37**, 1148 (1988).
- ⁹C. J. Horowitz and J. Piekarewicz, *Phys. Rev. Lett.* **62**, 391 (1989).
- ¹⁰J. R. Shepard, E. Rost, C.-Y. Cheung, and J. A. McNeil, *Phys. Rev. C* **37**, 1130 (1988).
- ¹¹A. L. Fetter and J. D. Walecka, *Quantum Theory of Many-Particle Systems* (McGraw-Hill, New York, 1971), and references therein.
- ¹²J. R. Comfort, computer code DW81, modification of DW70, R. Schaeffer and J. Raynal (unpublished); J. Raynal, *Nucl. Phys.* **A97**, 572 (1967).
- ¹³E. Rost and J. R. Shepard, computer code DREX (unpublished); E. Rost and J. R. Shepard, *Phys. Rev. C* **35**, 681 (1987).
- ¹⁴R. Smith, *Proceedings of the International Conference on Spin Observables of Nuclear Probes, Telluride, 1988* (Plenum, New York 1989).
- ¹⁵See, e.g., J. R. Taylor, *Scattering Theory: The Quantum Theory of Nonrelativistic Collisions* (Krieger, Malabar, 1983).
- ¹⁶E. Rost and J. R. Shepard, computer code DR1A (unpublished); J. R. Shepard, E. Rost, and J. Piekarewicz, *Phys. Rev. C* **30**, 1604 (1984).
- ¹⁷R. A. Eisenstein and G. A. Miller, *Comput. Phys. Commun.* **11**, 95 (1976).
- ¹⁸P. D. Kunz, code DWUCK4, University of Colorado (unpublished).
- ¹⁹J. L. Ullmann *et al.*, *Phys. Rev. C* **31**, 177 (1985).
- ²⁰C. Rowe, M. Salomon, and R. H. Landau, *Phys. Rev. C* **18**, 584 (1978).
- ²¹D. S. Oakley, M. R. Braunstein, J. J. Kraushaar, R. A. Loveman, R. J. Peterson, D. J. Rilett, and R. L. Boudrie, *Phys. Rev. C* **40**, 859 (1989).
- ²²Y. Torizuka, K. Itoh, Y. M. Shin, Y. Kawazoe, H. Matsuzaki, and G. Takeda, *Phys. Rev. C* **11**, 1174 (1975).
- ²³D. H. Youngblood, P. Bogucki, J. D. Bronson, U. Garg, Y.-W. Lui, and C. M. Rozsa, *Phys. Rev. C* **23**, 1997 (1981).
- ²⁴S. Drozd, V. Klemt, J. Speth, and J. Wambach, *Phys. Lett.* **166B**, 18 (1986); J. Wambach, S. Drozd, A. Schulte, and J. Speth, *Phys. Rev. C* **37**, 1322 (1988).
- ²⁵R. D. Smith and J. Wambach, *Phys. Rev. C* **38**, 100 (1988).
- ²⁶E. Rost and J. R. Shepard, computer code DRPA (unpublished).